An International Observation Campaign for a Study of Interhemispheric Coupling Initiated by Sudden Stratospheric Warmings in the Arctic

*Kaoru Sato[1], Yoshihiro Tomikawa[2,3], Masaki Tsutsumi[2,3], Masashi Kohma[1], Koji Nishimura[2,3]

1.Department of Earth and Planetary Science, Graduate School of Science, The University of Tokyo, 2.National Institue of Polar Research, 3.The Graduate University for Advanced Studies

Recent observational and modelling studies suggest that the Northern and Southern Hemispheres of the earth atmosphere are potentially coupled by the Lagrangian mean flow in the mesosphere modulated by waves interacting with the mean flow. However, observations of modulated wave and flow fields which are needed for quantitative understanding of the interhemispheric coupling are not sufficient. Simultaneous observations of gravity waves at various locations are most important because they are a main driver of the Lagrangian mean flow in the mesosphere.
With the start of full system observation by the PANSY radar in the Antarctic in March 2015, a global mesosphere-stratosphere-troposphere (MST) radar network extending from the Arctic to the Antarctic has been realized. The MST radars are able to observe wind vectors with fine temporal and vertical resolutions including vertical wind components in the troposphere, stratosphere and mesosphere, although an observational gap of the middle and upper stratosphere remains. Thus, the characteristics of small-scale or short-period wave motions including gravity waves and the momentum fluxes associated with these waves can be estimated with a good accuracy.
In addition, recent high-resolution general circulation models enable an explicit simulation of gravity waves under ideal and/or climatological boundary conditions and allow us to examine the momentum budget in the MST region including gravity waves, although their resolution is currently not sufficient to resolve the entire gravity wave spectrum. Real atmosphere simulations utilizing such high-resolution models are still a challenge for the MST region. However, if such real atmosphere simulations are successful, they will help quantitative interpretation of the dynamical fields observed by the MST radar network, and the observations will provide invaluable validation data for the model improvement.
Therefore we will examine the interhemispheric coupling of the earth atmosphere through a combination of simultaneous observations by networking the MST radars over the world and high-resolution model simulations of the observed atmosphere. This is an official project, ICSOM, for SCOSTEP, but it is closely related to SPARC. The first international observation campaign was successfully performed during a time period from 22 January-17 February, 2016 when two minor warming occurred in the Arctic stratosphere. Seven MST radars and many other radars and optical instruments providing complementary observational data were operated. More than 30 scientists in eight countries are participated in this project. A preliminary result from this observation campaign will be presented.

Keywords: interhemispheric coupling, middle atmospehre, sudden stratospheric warming, gravity waves, mesosphere-stratospehre-troposphere radars, general circulation

Characteristic of Vertical Winds Fluctuations in the Lower Troposphere at Syowa Station in the Antarctic Revealed by the PANSY Radar

*Yuichi Minamihara[1], Kaoru Sato[1], Masaki Tsutsumi[2], Masashi Kohma[1]

1.Department of Earth and Planetary Science Graduate School of Science The University of Tokyo, 2.National Institute of Polar Research and The Graduate University for Advanced Studies

Using wind data over three years from July 2012-June 2015 from the PANSY radar, an MST radar, newly installed at Syowa Station (39.59°E, 69.0°S), statistical characteristics of vertical winds and vertical momentum fluxes in the Antarctic lower troposphere are examined. Frequency spectra covering a wide frequency range from $(30\ \mathrm{d})^{-1}$ to $(8\ \mathrm{min})^{-1}$ are divided into three frequency regions obeying power laws with different scaling exponents. The transition frequencies are different between horizontal and vertical wind spectra. Vertical fluxes of horizontal momentum and variances of vertical wind were estimated for two wave period ranges of 1 d-2 h and 2 h-8 min having almost equal logarithmic scales. The momentum fluxes are larger for longer period components, and the variances of vertical wind disturbances are larger for shorter period component than longer period component. There are a few evidences showing that the vertical wind disturbances in the lower troposphere are due to gravity waves forced by topography aligned the north-south direction. First, the strong disturbances are observed when horizontal winds are strong near the surface. Second, zonal winds tend to almost zero around the top of the disturbances. Third, frequency spectra are large at a wide range of frequency below a critical level, as is consistent with the phase modulation of mountain waves by unsteady mean flow.

Keywords: MST Radar, Polar Atmosphere

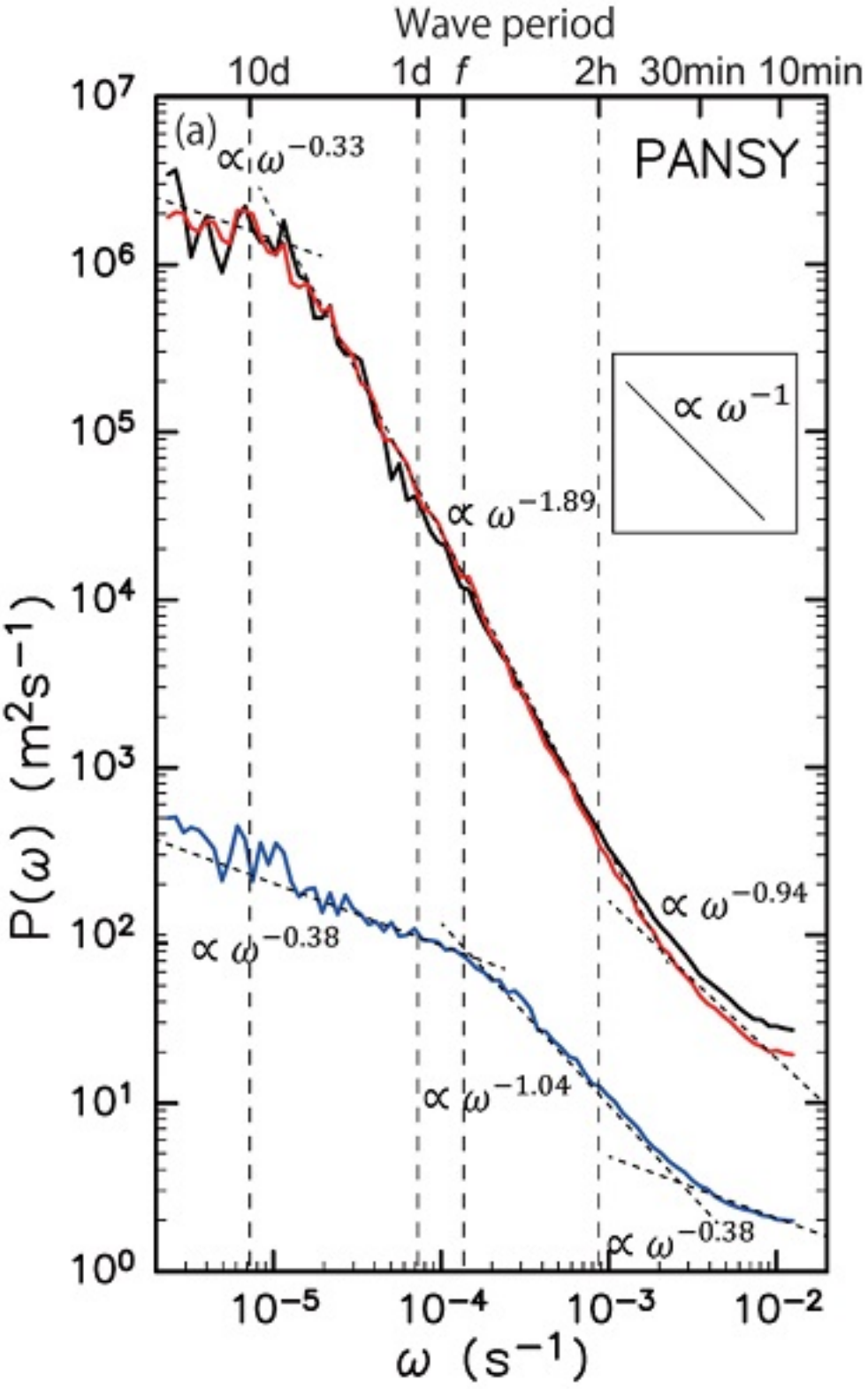

Figure : The frequency power spectra of zonal wind (black), meridional wind (red), and vertical wind (blue) fluctuations by PANSY radar. Both axis are log-scale.

Inertia-gravity waves in the mesosphere observed by the PANSY radar

*Ryosuke Shibuya[1], Kaoru Sato[1], Masaki Tsutsumi[2,3], Yoshihiro Tomikawa[2,3], Toru Sato[4], Koji Nishimura[2], Takuji Nakamura[2], Masashi Kohma[1]

1.Graduate School of Science, The University of Tokyo, 2.National Institute of Polar Reserch, 3.University for Advanced Studies (SOKENDAI), 4.Department of Communications and Computer Engineering, Kyoto University

The PANSY (Program of the Antarctic Syowa MST/IS radar) radar installed at Syowa Station (39°E, 69° S), the first MST/IS radar in the Antarctic, provides vertical profiles of three-dimensional wind vectors with fine height and time resolutions in the troposphere, stratosphere and mesosphere. We performed the first successful observation with a complete system of the PANSY radar in 16–24 March 2015. During this observation period, strong wave-like wind disturbances propagating phases downward were observed in the mesosphere. Their zonal wind amplitudes, vertical wavelengths and vertical phase velocities were estimated at about 30 m/s, 13 km and −0.3 m/s, respectively. This means that wave periods are about 11 h. We newly developed a grid configuration which were fine and equally-spaced only for high latitudes of the Southern Hemisphere, and performed a simulation using NICAM (a Nonhydrostatic ICosahedral Atmospheric Model) with the newly-developed grids. We successfully simulated strong wind disturbances similar to the PANSY radar observations with wave periods from 10–13 h in the mesosphere. First we examined amplitudes of the diurnal and semi-diurnal migrating tidal components and those of gravity wave components with horizontal wavelengths smaller than 1000 km as frequently examined by previous studies in the model-simulated wind field. Their amplitudes were much smaller than the observation, suggesting that dominant wave-structures in the mesosphere were not due to migrating tides nor small-scale gravity waves. The remaining components have quite similar structure and amplitudes to the observations. We estimated wave parameters of five dominant wave packets simulated near Syowa Station. Wave parameters of each wave packet were estimated as was consistent with the linear theory of hydrostatic inertia-gravity waves. Horizontal wavelengths are about 2000 km, which is also consistent with those estimated for the wavelike disturbances observed by the PANSY radar assuming that they are due to inertia-gravity waves. We examined propagation and sources of these wave packets using backward ray tracing method. It was suggested that a wave packet simulated at 00 UTC 19 March at 40° E in the mesosphere was generated by spontaneous radiation from the imbalance of polar night jet at the height of 50 km, while a wave packet simulated at 09 UTC 21 March at 120° W in the mesosphere was generated by spontaneous radiation from the imbalance of polar front jet at the tropopause.

Keywords: Atmospheric gravity waves, mesosphere

A study on data assimilation using the ensemble Kalman filter and simulation of a sudden stratospheric warming

*Dai Koshin[1], Kaoru Sato[2], Kazuyuki Miyazaki[3]

1.Department of Earth and Planetary Science, School of Science, The University of Tokyo, 2.Department of Earth and Planetary Science, The University of Tokyo, 3.Japan Agency for Marine-Earth Science and Technology

There are many important phenomena in the middle atmosphere, such as sudden stratospheric warmings (SSW), and the quasi-biennial oscillation (QBO). It is suggested that these phenomena affect global atmosphere through stratospheric and mesospheric circulations respectively from the equator to the pole and from the summer pole to the winter pole. With the aid of technology development, resolutions of observations and numerical models have become higher. Most analysis data are mainly made by meteorological centers by assimilating observation data up to the stratosphere. Data assimilation for the mesosphere is not yet very common. Thus, we performed a preliminary study for the data assimilation from the ground to the mesosphere, so as to make realistic grid data and simulation of the middle atmosphere.
First, using a global model called MIROC, whose top is in the upper stratosphere (~40km), we examined impacts of assimilation of satellite observations in the stratosphere. The PREPBUFR data (ground-based observations including these by aircrafts, balloons, and wind profilers) data from NCEP, and temperature retrieval data in the stratosphere by Aura MLS from NASA were used as conventional and satellite observations, respectively. The model has horizontal resolution of T42 and 32 vertical levels. We used the method of ensemble Kalman filter (EnKF) for data assimilation, and made analysis data for January and February 2014, when an SSW occurred in the northern hemisphere. As SSWs are highly non-linear phenomena, their simulation is generally difficult.
We made two kinds of analysis data. One is the data in which only PREPBUFR data are assimilated, and the other in which both PREPBUFR and MLS data are assimilated. In both analysis data, timing of the SSW onset was realistic. However, the data with MLS observation have higher accuracy in the middle atmosphere than that only with PREPBUFR data. It is seen from standard deviation of ensemble members that assimilation of satellite data is more effective (i.e. small standard deviation) in the stratosphere.
Second, we made ensemble forecast experiments using analysis data on February 1, several days before the SSW onset. The prediction using analysis data assimilated with both MLS and PREPBUFR was more accurate than that assimilated only with PREPBUFR. It is seen that there is significant difference in the stratospheric wave activity between the two prediction experiments, although the tropospheric wave activity is not so different. This fact suggests that accurate background fields around the tropopause are important so as to simulate realistic propagation of planetary waves from the tropopause to the stratosphere. For future studies, we will optimize each parameter at data assimilation, and use a hi-top model so that highly accurate data assimilation can be made in the middle atmosphere.

Keywords: data assimilation, sudden stratospheric warming, ensemble Kalman filter

Comparison of large-scale dynamical variations in the extratropical stratosphere among the JRA-55 family datasets

*Masakazu Taguchi[1]

1.Aichi University of Education

This study seeks to compare the “JRA-55 family” datasets in terms of the extratropical stratospheric and tropospheric circulation in both hemispheres. In particular, we explore large-scale dynamical variations such as stratospheric sudden warmings (SSWs) during NH winter and SH spring when the extratropical stratosphere is dynamically active.
The JRA-55 family consists of three datasets: a main product of the JRA-55 reanalysis data (referred to as STDD below), and two sub-products of JRA-55C and JRA-55AMIP (referred to as CONV and AMIP, respectively). CONV assimilates only conventional observations, whereas AMIP runs the same numerical weather prediction (NWP) model without assimilation of observational data. Kobayashi et al. (2014) reported preliminary results from these data, such as cold bias in the SH winter upper stratosphere (i.e., strong polar night jet bias) for CONV and AMIP compared to STDD.
Our comparison of AMIP to STDD reveals characteristic features of AMIP in frequency and vortex morphology of major SSWs during NH winter: AMIP shows a much smaller frequency, and has only vortex displacement events. These differences are contributed by two factors. First, the fixed threshold, or zonal wind reversal, for the major SSWs is disadvantageous to AMIP where the polar night jet is strong more often. Furthermore, the zonal wind response to planetary wave activity bursts in the lower stratosphere of a similar strength is weaker in AMIP than in STDD. This is particularly the case when wave 2 plays an important role. As for SH spring, large variability occurs later in AMIP than in STDD; e.g., AMIP exhibits no zonal wind reversal before late October
It is also found that CONV reproduces most of the DJF major SSWs identified in STDD, although some cases are identified a few days later or missed. In SH spring, CONV misses the major SSW in September 2002, as it, albeit slightly, underestimates the zonal wind deceleration. These differences of CONV would be understood by the bias of the NWP model (as seen in AMIP) and the paucity of data assimilation as hypothesized by Kobayashi et al. (2014).

Keywords: JRA-55 family datasets, Stratospheric sudden warmings

Formation of two dimensional and three dimensional circulation responding to unsteady wave forcing in the middle atmosphere

*Yuuki Hayashi[1], Kaoru Sato[1], Yuki Yasuda[1]

1.School of science, The Univercity of Tokyo

Lagrangian-mean meridional circulation in the middle atmosphere is important for the earth climate because it globally transports minor species such as ozone and changes the temperature structure through adiabatic heating/cooling associated with its vertical branches. This meridional circulation is mainly driven by remote redistribution of the momentum by atmospheric waves. In many previous studies such as Haynes et al. (1991), a steady-state assumption is frequently used for the analysis of the meridional circulation. In general, however, the wave forcing is not steady. Thus, dynamical understanding under the steady-state assumption is limited. When a stratospheric sudden warming occurs, for example, time scales of wave forcing is so short that behavior of the resultant circulation may differ from that expected under the steady-state assumption. So as to understand such transient behavior and formation of the circulation, we must investigate the time evolution of not only “slow” variable (linearized potential vorticity) but also “fast” variables such as horizontal divergence and ageostrophic vorticity. The purpose of this study is to theoretically examine the response of meridional circulation to unsteady wave forcing. In the first part of this study, we examine a two-dimensional problem using a Boussinesq equation system in which a zonally-uniform unsteady forcing is given. In the second part, the three-dimensional response to a zonally-nonuniform and unsteady forcing is examined using a balance equation which is derived in this study.

As large-scale atmospheric response to the forcing can be described as a linear response, the method of Green’s function, which is a response to the delta function, is one of useful approaches for analysis of the linear response to forcing. By using the Green's function method, we mainly examine the response to a wave forcing in the zonal momentum equation.

First, we investigate the response to the zonally-uniform forcing. The steady solution of the meridional circulation responding to a constant forcing is composed of two cells in the vertical. For a forcing with a shaped of the step function in time, gravity waves are radiated as a transient response, and a meridional circulation with an inertial oscillation finally remains. The quasi-steady meridional circulation accords well with the steady state solution for a constant forcing. The time scale needed for the formation of the meridional circulation depends on the aspect ratio of the wave forcing structure, as is consistent with a theoretical expectation. In addition, it is shown that the group velocity of gravity waves and the spatial scale of the forcing determine the time scale of the circulation formation. We also investigate the case for the forcing which changes gradually in time. When the forcing time change is slower than the inertial period, the meridional circulation always accords with that estimated using the “steady-state assumption”. The distribution ratio of the wave forcing to the zonal-wind acceleration and the Coriolis torque is also investigated. The distribution ratio is determined by the shape of the wave forcing and explained by the dimensional analysis.

Second, we investigate the response to zonally-nonuniform forcing. In this case, it is expected that Rossby waves are radiated as transient response because of beta effect. So as to focus only on the Rossby wave response, governing equations are derived following the method of balance equations used by Leith (1980). For the steady forcing case with beta effect, the geostrophic flow becomes zonally asymmetric and has large magnitudes to the west of the forcing. For the step-function forcing, Rossby waves are radiated as a transient response. Rossby waves having smaller zonal wave

numbers radiated faster from the forcing region. Time period needed to reach the steady state depends strongly on the strength of the linear relaxation.

Keywords: middle atmosphere, circulation, wave forcing

A study of three dimensional structure of stratospheric material transport and ozone

*Takenari Kinoshita[1], Kaoru Sato[2]

1.National Institude of Information and Communications Technology, 2.Department of Earth and Planetary Science, Graduate School of Science, The University of Tokyo

The Transformed Eulerian-Mean (TEM) equations have been widely used to examine wave-mean flow interaction in the meridional cross section. According to previous studies, the Brewer-Dobson circulation in the stratosphere is driven by planetary waves, baroclinic waves, and inertia-gravity waves, and that the meridional circulation from the summer hemisphere to the winter hemisphere in the mesosphere is mainly driven by gravity waves. However, the TEM equations do not provide the three-dimensional view of the transport, so that the three dimensional TEM equations have been formulated. On the other hand, the TEM equations cannot properly treat the lower boundary and unstable waves. The Mass-weighted Isentropic Mean (MIM) equations are the equations that overcome those problems and the formulation of three-dimensional MIM equations have been studied. The present study applies the three-dimensional TEM and MIM equations to the ERA-Interim reanalysis data and examines the three-dimensional structure of Stratospheric Brewer-Dobson circulation. Next, we will discuss material transport due to disturbances on the distribution of stratospheric ozone.

Keywords: residual mean flow, ozone, meridional circulation

Three dimensional structure of mean meridional circulations and their forcing

*Yuki Kanno[1], Toshiki Iwasaki[1]

1.Tohoku University

The zonal mean meridional circulation in the stratosphere is called Brewer-Dobson circulation (BDC). It transports air masses upward in the tropics, poleward in mid-latitudes, and downward in the extratropics. In the winter troposphere, direct circulation is depicted in the extratropics by isentropic zonal means. However, longitudinal variation of these circulations is not fully understood. This study examines the three dimensional structure of BDC and extratropical direct (ETD) circulation based on mass-weighted isentropic time mean method.
The mass-weighted isentropic time mean method expands Mass-weighted isentropic zonal means (Iwasaki, 1989) longitudinally by substituting the time means for the zonal means. The longitudinal variation of the BDC and ETD circulation are depicted by mass-weighted isentropic time mean meridional winds and temporal change of potential temperature. The zonal momentum equation of the mass-weighted isentropic time mean is composed of Coriolis term, advection term, Eliassen-Palm flux (EP flux) divergence term, and residual term. The EP flux divergence term can be divided into form drag terms by stationary and transient waves and reynolds stress term. A momentum budget analysis shows the forcing term of mean meridional circulations.
Mass-weighted time mean meridional winds at 45N take a wave-number three pattern in the troposphere and a wave-number two pattern in the stratosphere. Compared with time mean meridional wind in pressure coordinates, it has strong northerly wind in the lower troposphere, which indicates time mean cold air outbreak from the northern high latitudes. The geographical patterns of the meridional winds are similar in the stratosphere. The momentum budget analysis shows that the form drag term induced by the stationary waves is almost balanced with the Coriolis term.

Keywords: Meridional circulation, Isentropic coordinate

Dynamical characteristics of mesoscale disturbances around Asian monsoon anticyclone and its influence on Stratosphere-Troposphere exchange

*Arata Amemiya[1], Kaoru Sato[1]

1.Graduate School of Earth and Planetary Science, Tokyo University

Recent studies on the stratosphere-troposphere exchange of tracers have focused on the importance of the Asian monsoon anticyclone (hereafter 'AMA'), which is planetary-scale, thermally driven circulation dominating the upper troposphere and lower stratosphere (UTLS) over South and Southeast Asia (Randel et al., 2010). On 360-380K isentropic surfaces, in most cases, the AMA is surrounded by a boundary between the tropospheric air inside and the stratospheric air outside. Isentropic mixing between inside and outside the AMA is suppressed by the strong anticyclonic circulation, which corresponds to the maximum in PV gradient acting as a mixing barrier (Ploeger et al., 2015). On the other hand, the AMA itself has a large intra-seasonal variability including synoptic-scale disturbances and vortex-shedding due to instability (Popovic and Plumb, 2001), which are probably essential processes that lead to irreversible mixing. In this study, we explore dynamical characteristics of synoptic-scale disturbances around the AMA, focusing on a vertical flow.
We used ERA-Interim reanalysis data for June-September, 2011-2015 with the horizontal resolution 1.5^{o}x1.5^{o}. Because of possible large differences in the UTLS region among reanalysis data sets, we also performed the same analyses using JRA55 and MERRA to confirm the results.
First, the intermittent nature of the occurrence of a large PV air in 5-20^{o}N on the southern flank of the AMA is confirmed. The air with large stratospheric PV is formed as an occasional cutoff of mid-latitude stratospheric air and is advected from the northeastern part of the AMA ('in-mixing'). The positive anomalies of PV averaged over 0-20^{o}N on 370K decay gradually during westward migration, suggesting that in-mixing is essentially irreversible. Thus, we next focus on individual events of PV disturbances and associated meridional circulation, which is likely important for the irreversible diabatic mixing.
On 150 hPa level, it seems that most high PV anomalies appear with a downward flow. This feature can be understood as a low-latitude version of a well-known tropopause descent around a westerly jet, which is seen also on the northern flank of the AMA. Similar results are obtained from different reanalysis data.
Next, this characteristic vertical flow pattern is examined from a perspective of the balanced jet dynamics. Even in the low latitude UTLS region, the horizontal flow roughly satisfies the geostrophic balance because it is dominated by easterly jet. This means that the meridional circulation on a plane perpendicular to the geostrophic wind can be diagnosed using the Sawyer-Eliassen equation, which is based on a balanced-jet approximation (Hoskins, 1975).

$$N^2 \partial^2\psi/\partial y^2+2S^2 \partial^2\psi/\partial y \partial z+Fs^2(\partial^2\psi/\partial z^2-\psi/4H^2)=Q_y$$

Note that Q_y is regarded as the forcing by the balanced flow. A previous study on the tropopause folding around the cold-front jet (Uccelini et al., 1985) successfully reproduced a spatial pattern of the meridional flow using this equation. On the northern flank of the AMA, a similar pattern of Q_y is observed around the meandering jet, which is characterized as a vertical dipole across the jet exit region. However, on the southern flank, Q_y is not always consistent with the vertical flow pattern. Instead, we found that it can be explained as moist symmetric instability. Figure 1 shows snapshots of PV, vertical flow, equivalent potential temperature and absolute angular momentum. Isopleths of the latter two quantities are inclined southward closely each other around 15^{o}-25^{o}N, 125-250hPa. This implies the existence of oblique instability forming a vertical flow pattern observed near the tropopause.

Keywords: Atmospheric dynamics, Stratosphere-Troposphere coupling, Tracer transport and mixing

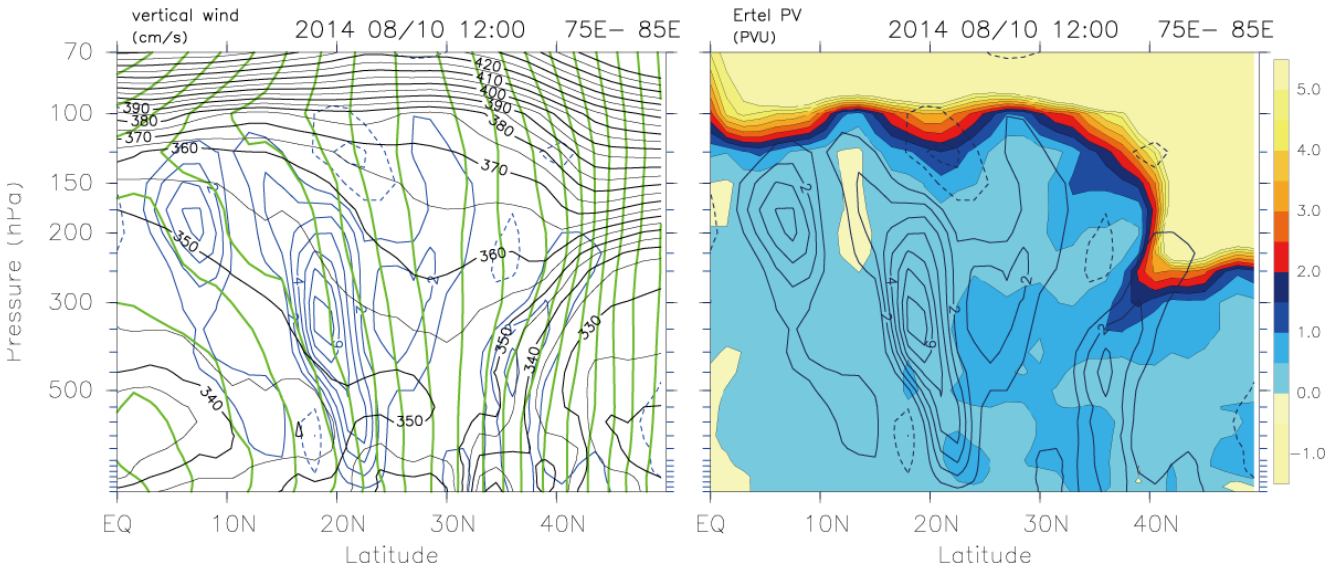

Spatial and temporal variations of atmospheric methane concentration and its carbon and hydrogen isotopic ratios in the upper troposphere/lower stratosphere over the Eurasian continent observed by commercial airliner

*Ryo Fujita[1], Shinji Morimoto[1], Shuji Aoki[1], Toshinobu Machida[2], Yousuke Sawa[3], Hidekazu Matsueda[3], Yosuke Niwa[3], Kazuhiro Tsuboi[3], Keiich Katsumata[2], Takakiyo Nakazawa[1]

1.Center for Atmospheric and Oceanic Studies, Graduate School of Science, Tohoku University, 2.National Institute for Environmental Studies, 3.Meterological Research Institute

Aircraft observation campaigns over the northern high latitudes have been conducted to clarify the spatial and temporal variations of GHGs concentrations and their sources in the surfaces (Sugawara et al., 1996; Tohjima et al., 1997; Nakazawa et al., 1997; Paris et al., 2008); however, systematic time-series observations using aircrafts are still limited (Matsueda et al., 2002; Haszpra et al., 2012; Umezawa et al., 2012). In addition, there is no systematic and simultaneous observation for the atmospheric CH_4 concentrations and their isotopic ratios ($\delta^{13}C$, δD) in the upper troposphere/lower stratosphere over the northern high latitudes; except for a few studies using balloon flights and aircraft observation campaigns (Sugawara et al., 1997; Rice et al., 2003; Rö ckmann et al., 2011). In this study, we have conducted monthly air sampling on-board a commercial airliner between Europe and Japan from April 2012, and clarified the spatiotemporal variations of CH_4, $\delta^{13}C$ and δD in the upper troposphere/lower stratosphere over the Eurasian continent.
In the upper troposphere, CH_4 concentrations, $\delta^{13}C$ and δD showed no clear seasonal variations. In the lower stratosphere, on the other hand, CH_4 and $\delta^{13}C$, δD showed clear aniti-phase seasonal variations; seasonal maximum (minimum) of the CH_4 concentration ($\delta^{13}C$, δD) was found in November to January and seasonal minimum (maximum) was in spring. They can be explained by effective flushing of the lowermost stratospheric air with the tropospheric air in autumn and subsidence of the middle stratospheric air in spring (Sawa et al., 2015). Moreover, compact correlations of CH_4 with respect to $\delta^{13}C$ and δD were found in the lower stratosphere, suggesting the occurrence of reactions of CH_4 not only with OH, but also with Cl and $O(^1D)$.

Keywords: Methane, carbon and hydrogen isotopic ratios, upper troposphere/lower stratosphere, Eurasian continent

CO_2 and SF_6 concentrations in the stratosphere over Indonesia

*Satoshi Sugawara[1], Shuji Aoki[2], Shinji Morimoto[2], Shigeyuki Ishidoya[3], Takakiyo Nakazawa[2], Sakae Toyoda[4], Chusaku Ikeda[5], Hideyuki Honda[5], Yoichi Inai[6], Fumio Hasebe[6], Fanny Aditya Putri[7], Daisuke Goto[8]

1.Miyagi University of Education, 2.Tohoku University, 3.AIST, 4.TITECH, 5.JAXA/ISAS, 6.Hokkaido University, 7.LAPAN, 8.NIPR

Stratospheric air collections were carried out at Biak, Indonesia in February 2015, by using the compact cryogenic air sampler (J-T sampler). Eight sets of air sampler were launched from the experiment field in LAPAN observatory (001°10'32" S, 136° 06'02" E) using 4 large plastic balloons. The data obtained at 8 different altitudes will be used for elucidating the vertical structures of GHGs and their chemical processes in the TTL and the tropical stratosphere, with an average vertical resolution better than 2km. Air samples were analyzed for concentrations of CO2, CH4, N2O, and SF6 at Tohoku University and Miyagi University of Education. The concentrations of CO2 and SF6 at 29 km altitude were 392.9 ppmv and 7.5 pptv, respectively. Stratospheric CO2 and SF6 are known as the ‘clock tracer’. In this study, we estimated the mean age of air in the tropical stratosphere over Biak, and compared them with the results obtained from the previous experiments at Japan, Kiruna, and Syowa station. The CO2 concentration data was corrected for the airborne production by methane oxidation. CO2- and SF6-age were estimated by comparing the observed concentrations with the CONTRAIL data records in the tropical upper troposphere. As a result, the mean age of air was estimated to be about 3 years at 29km altitude. This value was significantly lower than those obtained from the satellite SF6 measurements.

Keywords: CO2, SF6, Age of air

Diffusive separation of major atmospheric components in the stratosphere over Indonesia

*Shigeyuki Ishidoya[1], Satoshi Sugawara[2], Shuji Aoki[3], Shinji Morimoto[3], Takakiyo Nakazawa[3], Sakae Toyoda[4], Chusaku Ikeda[5], Hideyuki Honda[5], Yoichi Inai[6], Fumio Hasebe[6], Fanny A. Putri[7], Daisuke Goto[8], Shohei Murayama[1]

1.National Institute of Advanced Industrial Science and Technology (AIST), 2.Miyagi University of Education, 3.Tohoku University, 4.Tokyo Institute of Technology, 5.Japan Aerospace Exploration Agency (JAXA), 6.Hokkaido University, 7.Lembaga Penerbangan dan Antariksa Nasional (LAPAN), 8.National Institute of Polar Research

In the atmosphere over the turbopause (about 100 km), the mole fraction of heavier molecules decreases with increasing altitude due to diffusive separation in Earth's gravitational field. Recently, Ishidoya et al. (2013) reported such gravitational separation of the atmosphere is also found in the middle to lower stratosphere (about 15-35 km) over Japan from high precision measurements of the composition of the atmospheric major components. To investigate whether gravitational separation is also detectable over the equatorial region or not, we carried out collection of the stratospheric air using a balloon-borne cryogenic air sampler over Biak, Indonesia during February 22-28, 2015. For the observation, we used a Joule-Thomson minicooler, developed by Morimoto et al. (2009), as the cryogenic air sampler, and succeeded to collect 8 air samples at heights of 17-29 km. The collected air samples were analyzed for delta(Ar/N_2), delta(O_2/N_2), delta^{15}N of N_2, delta^{18}O of O_2 and delta^{40}Ar by using a mass spectrometer (Ishidoya and Murayama, 2014), and the measured values showed small but significant decrease with altitude probably due to gravitational separation. The amount of gravitational separation, evaluated as delta values for the mass number difference of 1 (e.g. delta for $^{15}N^{14}N/^{14}N^{14}N$), is found to be 11 per meg at the height of 29 km. Based on the observed gravitational separation and a 1-dimensional steady state eddy diffusion/molecular diffusion model, we estimated 1-dimensional vertical eddy diffusion coefficients (K_z) over the equatorial region. By using the average K_z from the surface to the middle stratosphere, we calculated a timescale of the vertical diffusion for a length scale from the surface to the middle stratosphere assuming simple Fickian diffusion. We found that the calculated timescale agrees with the elapsed time since the stratospheric air passed an upper boundary of the tropical tropopause layer (TTL), estimated from tape recorder signals of stratospheric water vapor (Mote et al., 1996), which is significantly smaller than the mean age of air estimated from CO_2 concentration (CO_2 age). This discrepancy may be due to insensitivity of gravitational separation to mixing processes in Brewer-Dobson circulation, of which variations change the mean age of air significantly.

References

Ishidoya, S. et al. (2013) Gravitational separation in the stratosphere –a new indicator of atmospheric circulation. *Atmos. Chem. Phys.*, 13, 8787–8796, www.atmos-chem-phys.net/13/8787/2013/, doi:10.5194/acp-13-8787-2013.

Ishidoya, S. & Murayama, S. (2014) Development of high precision continuous measuring system of the atmospheric O_2/N_2 and Ar/N_2 ratios and its application to the observation in Tsukuba, Japan. *Tellus B*, 66, 22574, http://dx.doi.org/ 10.3402/tellusb.v66.22574.

Morimoto et al. (2009) A new compact air sampler and its application in stratospheric greenhouse gas observation at Syowa station, Antarctia. *J. Atmos. Oceanic and Technol.*, 26 10.1175/2009JTECHA1283.1.

Mote, P. W. et al. (1996) An atmospheric tape recorder: The imprint of tropical tropopause temperatures on stratospheric water vapor. *J. Geophys. Res.*, 101, 3989-4006.

Keywords: gravitational separation of atmospheric components, cryogenic air sampler, stratosphere over Indonesia

Observational study of the short-lived ozone depleting substances, bromoform and dibromomethane

*Yoko Yokouchi[1], Takuya Saito[1], Jiye Zeng[1], Hitoshi Mukai[1], Stephen Montzka[2]

1.National Institute for Environmental Studies, 2.National Oceanic and Atmospheric Administration

Bromoform ($CHBr_3$) and dibromomethane (CH_2Br_2), which undergo photolytic degradation and react with OH to produce inorganic bromine, are the large contributors of organic bromine from the ocean to the atmosphere, where it can affect stratospheric and tropospheric ozone chemistry (Carpenter and Liss 2000; Montzka and Reimann 2011). These naturally produced ozone-depleting substances (ODS) are attracting more interest as concentrations of anthropogenic ODS decrease under the provisions of the Montreal Protocol. The major sources of these bromocarbons are believed to be seaweed or macroalgae, followed by phytoplankton and other biological sources, but many uncertainties remain with regard to their production amount and mechanism. In this study, we conducted high-frequency long-term measurements of CH_2Br_2 and $CHBr_3$ at Hateruma Island, and found that the relationship between $[CH_2Br_2]/[CHBr_3]$ and $[CHBr_3]$ could be explained by their chemical decay in the atmosphere with a fairly consistent $CH_2Br_2/CHBr_3$ initial emission ratio, and some additional coastal effects. By combining these data with NOAA global observation data (14-yr monthly data from 14 ground stations), we obtained new insight into the global sources of these bromocarbons and their chemical degradation.

Keywords: bromocarbons, sources, long-term observation

Box-model simulation for atmospheric effect of solar energetic particles: variation of trace chemical species in the middle atmosphere

*Yoichi Nakai[1], Yuko MOTIZUKI[1], Manami MARUYAMA[1], Hideharu Akiyoshi[2], Takashi Imamura[2]

1.RIKEN Nishina Center, 2.National Institute for Environmental Studies

Recently, the atmospheric effect of solar energetic particles (SEPs) has attracted interests. High-energy protons in SEPs are able to come down to the stratosphere in the polar region and they are considered to induce increase of reactive odd nitrogen species (NOy) due to dissociation of nitrogen molecules. Furthermore, they cause depletion of ozone through the catalytic reaction cycle involving NOy over a period longer than SEP events. The concentration variations of several chemical species have been observed and their simulations have been attempted [1].
We have studied concentration variation of trace chemical species induced by SEP protons through the Box-model simulation. It involves multitudinous reactions of various ionic and neutral chemical species but no transport processes. We simulated the concentration variations for the middle atmosphere in polar region during the SEP event in October-November 2003. In this simulation, we adopt 77 chemical species and 522 gas-phase ionic and neutral reactions. We assume that the prompt products are charged and neutral species generated from nitrogen and oxygen molecules and that the yields of the prompt products are determined only with the energy deposit in the air. These prompt products generated by the SEP protons induce subsequent ionic and neutral chemical reactions (SEP-induced reactions). The production rates of the prompt products were estimated using the G-value [2,3]. The daily energy deposits were estimated from the calculated daily ion-pair creation rate due to the SEP protons [4]. The concentration variation of each species due to SEP protons was estimated as the difference between the result by considering both SEP-induced and photochemical reactions and that only for photochemical reactions under the same initial condition.
In this talk, we will mainly report the results of our simulation for the variations of ozone and reactive odd nitrogen species for the SEP event in October-November 2003.

References
[1] For example, B. Funke *et al.*, Atmos. Chem. Phys. 11, 9089 (2011).
[2] C. Willis and A. W. Boyd, Int. J. Radiat. Phys. Chem. 8, 71 (1976).
[3] H. Mätzing, Adv. Chem. Phys. LXXX, 315 (1991).
[4] C.H. Jackman *et al.*, Atmos. Chem. Phys. 8, 765 (2008).

Characteristics of dynamical and chemical fields in Chemistry Climate Models

Takuya Sasaki[1], *Masato Shiotani[1], Hideharu Akiyoshi[2], Makoto Deushi[3], Douglas Kinnison[4]

1.Research Institute for Sustainable Humanosphere, Kyoto University, 2.National Institute for Environmental Studies, 3.Meteorological Research Institute, 4.National Center for Atmospheric Research

We analyzed results from three coupled chemistry-climate models (CCM) to investigate characteristics of climatological differences between free-running (FR) and specified dynamics (SD) modes, by paying attention to interactions between dynamical and chemical fields. The three models used in this study are the NCAR Whole Atmosphere Community Climate Model, version 4 (WACCM4) (Marsh et al., 2013), the Model for Interdisciplinary Research on Climate 3.2-Chemistry-Climate Model (MIROC3.2-CCM) (Imai et al., 2013; Sakazaki et al., 2013), and the Meteorological Research Institute-Earth System Model Version 1 Revision 1 (MRI-ESM1r1) (Deushi and Shibata, 2011; Adachi et al., 2013). Outputs from the three models are based on simulations proposed by IGAC/SPARC Chemistry-Climate Model Initiative (CCMI) to improve our understanding in modelling of the chemistry and dynamics of the troposphere and stratosphere. REF-C1 and REF-C2 simulations for FR mode CCM (FR-CCM) and REF-C1SD simulation for SD mode CCM (SD-CCM) are used for the period of 1980-2010 as monthly means.

We carefully analyzed differences found at mid-high latitudes in the stratosphere of the winter hemisphere, the extratropical upper troposphere and lower stratosphere (Ex-UTLS) and the tropical tropopause layer (TTL). Comparisons of stratospheric temperatures at mid-high latitudes show that for all FR-CCM results the seasonal change is delayed in both hemispheres during the winter and spring; especially in the southern hemisphere all FR-CCM results show cold biases in early spring. Results for ozone are similar to those for temperature, and the biases in the southern hemisphere are clearer than in the northern hemisphere. We also investigated the Eliassen-Palm fluxes (EP flux) and resulting residual mean meridional circulations, because the seasonal changes in temperature and ozone during these seasons and in those regions are affected by the meridional circulation. EP flux convergences and downward velocities in winter are smaller for all FR-CCM results than SD-CCM ones, indicating that the time of maximum wave activities seen in EP fluxes are delayed about 1-2 months for all FR-CCM results. These suggest that the temperature and ozone biases are due to some problems with model reproducibility of planetary waves propagating into the stratosphere from the troposphere.

In the Ex-UTLS, all FR-CCM results show cold biases especially in summer, and all SD-CCM results overestimate radiative cooling effects. Comparisons of water vapor with satellite observations (Aura-MLS) and models show that all model results overestimate water vapor in the upper troposphere at mid- and high latitudes. Because water vapor has an important role in the radiation budget during the summer in this region, the FR-CCM cold biases and the SD-CCM overestimations of radiative effects are from water vapor overestimations. The dynamical fields are specified in SD-CCM, therefore these overestimations are due to the model reproducibility of chemical, transport and microphysics processes associated with water.

In the TTL, we compared ozone distributions in SD-CCM and FR-CCM results. We found that FR-CCM of MIROC3.2-CCM and WACCM4 cannot reproduce the increase of ozone in boreal summer. This is due to the annual cycle of upwelling and the horizontal transport from mid latitude; this mechanism is called in-mixing and is understood as the nearly isentropic transport owing to the Asian and North American monsoon anticyclones. WACCM4 FR-CCM can reproduce this increase in isentropic coordinate, and the Asian monsoon anticyclone is weak in the FR-CCM of MIROC3.2-CCM. These indicate that

temperature and monsoon anticyclone reproducibility is strongly related to the improvement of ozone results in the TTL.

Keywords: Chemistry Climate Model, stratospheric dynamics and chemistry, extratropical upper troposphere and lower stratosphere, tropical tropopause layer

Future changes in quasi-biennial oscillation of ozone with increasing GHS and ozone recovery in CCMI simulation

*Hiroaki Naoe[1], Makoto Deushi[1], Kohei Yoshida[1], Kiyotaka Shibata[2]

1.Meteorological Research Institute, 2.Kochi University of Technology

The future quasi-biennial oscillation (QBO) in ozone in the equatorial stratosphere is examined by analyzing future transient reference simulation (REF-C2) for the period from 1960 to 2100 in a climate change due to increasing GHGs and decreasing ODSs under the Chemistry-Climate Model Initiative (CCMI) activities. The REF-C2 simulation is conducted using the Meteorological Research Institute Earth System Model (MRI-ESM), which constitutes a core component of the atmosphere-ocean coupled global climate model and components of sea-ice, aerosol, and ozone models. We have conducted the wavelet analysis to provide inter-annual variability of amplitude and phase of the ozone QBO in the vertical structure of tropical stratosphere.
In the simulation the power spectra of the equatorial zonal-mean ozone mixing ratio shows a double peak structure with maximum amplitude at two pressure levels of around 30 hPa and 10 hPa and a node at 15 hPa. The vertical residual-velocity anomalies are in phase with the ozone anomalies in the upper stratosphere with the abrupt phase change at around 15 hPa. Below this level, the phase is almost reversed from what it is above. Quantitatively, the amplitude of the ozone QBO in the model-free simulation (REF-C2) is reduced to 0.25 ppmv at 10 hPa, which is about half of that in the simulation forced by the meteorological reanalysis data (REF-C1sd).
Compared with the past climatology of 1960-1980 at the time before the severe ozone destruction, the amplitude of the future equatorial ozone QBO during the period of 2040-2070 at the time of the ozone recovery is characterized by the decrease by 20-30% at 30 hPa and the increase by around 20% at 5-10 hPa. This can be explained by the fact that the dominant role of future ozone decrease in the lower stratosphere is due to the changes in tropical upwelling. In addition, it is found that chemical ozone production and destruction do contribute to the ozone changes in the tropical upper stratosphere.

Keywords: ozone QBO, quasi-biennial oscillation, ozone depletion and recovery

Forcing and feedbacks of geoengineering by SO_2 injection into the stratosphere: Analysis of GeoMIP G4 experiment

*Hiroki Kashimura[1], Takashi Sekiya[2], Manabu Abe[1], Shingo Watanabe[1]

1.Japan Agency for Marine-Earth Science and Technology, 2.Graduate School of Environment Studies, Nagoya University

Geoengineering is a deliberate large-scale manipulation of the planetary environment to counteract anthropogenic climate change. Manners of geoengineering for lessening the effects of global warming can be classified into two groups. One is Solar Radiation Management (SRM), which aims to reduce the amount of solar radiation at the surface by increasing the reflection rate. The other is Carbon Dioxide Removal, which aims to reduce the amount of CO_2 in the atmosphere. One of the most probable approaches for SRM is to mimic a large volcanic eruption by injecting sulfate aerosol precursors, such as SO2, into the stratosphere. The sulfate aerosols increase the solar reflectance of the atmosphere, decrease the shortwave radiation (SW) reaching the surface, and cause cooling of surface air temperature. The Geoengineering Model Intercomparison Project (GeoMIP) was established to coordinate simulations with a common framework and to determine the robust effects and responses to geoengineering processes.
In this study, we analyze GeoMIP's G4 experiment, which is designed to inject SO_2 into the lower stratosphere at the equator by 5 Tg/year from 2020 to 2070 with adopting the RCP4.5 scenario as the baseline. This injection rate is about 1/4 of the 1991 eruption of Mount Pinatubo. Some participant models have explicitly calculated the formation of sulfate aerosols from SO_2 and their distribution; whereas some models have just used prescribed aerosol optical depth (AOD) based on the observed AOD after 1991 eruption of Mount Pinatubo. Therefore, a careful comparison is required. In addition, at least cloud amounts, water vapor amounts, and surface albedo can change because of the cooling of the air temperature by SRM. Changes of these amounts affect the reflection and absorption of SW and give some feedbacks to the effect of SRM.
To separately estimate the direct SRM forcing and the feedbacks on each model, we use a single layer atmospheric model for SW transfer. By using this model, we can derive the SW reflection and absorption rates of the atmosphere and surface albedo from the following model outputs: upwelling and downwelling SW at the surface and at the top of the atmosphere. In addition, these calculation can be done with whole-sky amounts and clear-sky amounts, and we can estimate the cloud effects by the their differences. Then, we calculate the contribution of each term described above to the change of net SW at the surface from RCP4.5 to G4, and estimate the direct SRM forcing and the feedbacks. Here, we assume that the change of clear-sky reflection rate is due to the injected sulfate aerosols and that of clear-sky absorption rate is due to the change of water vapor amounts.
Our analysis shows that the globally and temporally averaged SRM forcing ranges widely from -3.6 to -1.6 W/m^2 depending on the models. The SRM forcing on the models with sulfate aerosol calculation is significantly higher than that using the prescribed AOD. This means that the prescribed AOD might underestimate the SRM forcing by 5 Tg/year SO_2 injection. The feedback from cloud amounts and that from water vapor amounts are comparable and range from +0.5 to +1.5 W/m^2 (heating effects). The feedback from water vapor amounts is almost proportional to the cooling of the near-surface air temperature. On the other hand, the cloud feedback shows strong model dependency. The surface albedo feedback works for cooling but it is small (for averaged value).
Our results show the fact that, in the simulation of the geoengineering with SO_2 injection, the uncertainty of the SRM forcing itself is considerably large and that SRM forcing could be decreased by about 50% by the feedbacks from changes in cloud amounts, water vapor amounts, and surface

albedo.

Keywords: Geoengineering, Stratospheric aerosols, Shortwave radiation, GeoMIP

Effects of geoengineering by stratospheric SO_2 injection on stratospheric sulfate aerosols and circulation

*Takashi Sekiya[1], Hiroki Kashimura[2], Shingo Watanabe[2], Kengo Sudo[1,2]

1.Graduate School of Environmental Studies, Nagoya University, 2.Japan Agency for Marine-Earth Science and Technology

Geoengineering is deliberate manipulation of climate system to counteract anthropogenic climate change due to greenhouse gases. In the geoengineering techniques, stratospheric SO_2 injection is analogically based on SO_2 injection by explosive volcanic eruption and subsequent surface cooling. However, climate models participating in the Geoengineering Model Intercomparison Project (GeoMIP) demonstrate diverse results. Some of uncertainties of the results are aerosol microphysical properties and stratospheric circulation. This study introduces an aerosol microphysics module of stratospheric sulfate aerosols into the MIROC-ESM-CHEM earth system model (hereinafter, MIROC-ESM-CHEM-AMP). The model can represent aerosol microphysical properties and aerosol transport explicitly. We conducted the geoengineering simulation using MIROC-ESM-CHEM-AMP in the same manner as the GeoMIP's G4 experiment. G4 experiment assumes stratospheric SO_2 injection of 5 Tg/year into the lower stratosphere at the equator during 2020–2070 under RCP4.5 scenario. We also compare the results of MIROC-ESM-CHEM-AMP with the results of MIROC-ESM-CHEM. G4 experiment with MIROC-ESM-CHEM prescribes stratospheric aerosol optical depth (SAOD) based on the observed SAOD after the 1991 eruption of Mt. Pinatubo. The results show that SAOD in MIROC-ESM-CHEM-AMP is twice as large as SAOD in MIROC-ESM-CHEM. In MIROC-ESM-CHEM-AMP, the effective radius of stratospheric sulfate aerosols grew by 0.51 μm in the tropical lower stratosphere because of the stratospheric SO_2 injection. Mean residence time of stratospheric sulfate aerosols is 1.13 year. The stratospheric burden is 2.85 TgS that is larger than the yearly injected SO_2 amount (2.5 TgS).
This study also investigates effects of the stratospheric SO_2 injection on mean age of stratospheric air. In the both models, the stratospheric SO_2 injection increases the mean age by 0.15 year at maximum and decreases the mean age by 0.25 year at maximum. The changes in the mean age in MIROC-ESM-CHEM-AMP are more than three times as large as the changes in MIROC-ESM-CHEM. We furthermore assess the effects of the stratospheric SO_2 injection on the mean age of stratospheric air using the G4 experiment with sea surface temperature (SST) of the RCP4.5 experiment (without geoengineering). The results suggest that the increase in the mean age is caused by slow response (e.g., SST changes) and that the decrease is caused by fast response (e.g., longwave radiation absorption of sulfate aerosols). The model results also demonstrate that the slow response leads to weakened circulation in the lower stratosphere, resulting in a slight increase in SAOD (about 5%).

Keywords: Geoengineering, Stratospheric aerosols, Stratospheric circulation, Aerosol microphysics

Cloud classification based on histogram analysis of pixel values of night time cloud images over Manila Observatory (14.64N, 121.07E)

*GlennFranco Barroso Gacal[1,2], Nofel Lagrosas[1,2]

1.Manila Observatory, 2.Ateneo de Manila University

Satellites and ground based instruments are utilized to achieve cloud detection. At night time, detection of clouds is accomplished by satellites, whole-sky imagers, lidars, and sky cameras. In practice, ground-based detection is executed by sky cameras and whole-sky imagers and incorporating a threshold value into the analysis of cloud detection. This will classify pixels as clouds or non-clouds. In this work, we use a ground-based sky imager using a digital camera to take pictures of the sky. The digital camera (Canon Powershot A2300) is continuously operated to take images of night time clouds at 5 minute intervals. The camera is configured to have an exposure time of 1s and 5s and is situated on the roof top of the Manila Observatory building (14.64N, 121.07E). This is to ensure that there is a minimal presence of obstructions for the camera. A threshold value is applied to distinguish a pixel to be a cloud or non-cloud by analyzing the histogram of pixel values of clear sky. Other works use the similar procedure of applying a threshold value to detect clouds at daytime (Heinle et al., 2010). In this study, the RGB formatted images are converted to greyscale format. Lastly, an algorithm is applied to compute cloud occurrence (Gacal et al., *submitted*). Cloud occurrence is determined but not its corresponding cloud types: thin, thick, and cloud-free. The objective of this study is to determine these cloud types in terms of their range of pixel values. Figs. 1a -1c show the images of a clear night sky, thin clouds, and thick clouds, respectively. These images were taken on 16 January 2016, 21 October 2015, and 25 May 2014, respectively. From visual inspection, thick clouds (Fig. 1c) are perceived to have no distinguishable dark background as compared to the thin clouds (Fig. 1b). Figs. 1a –1c are taken at 1s exposure time except Fig. 1a with an exposure time of 5s. Figs. 1d –1f show the histogram of each corresponding cloud type. The histogram of a cloud free sky (Fig. 1d) presents the pixel values that range from 0 –16. This implies that a minimal pixel value of 17 can be used to discriminate the presence and absence of clouds of a night sky (Gacal et al., *submitted*). Comparing this to Fig 1e, this histogram shows a superposition of a clear sky and thin clouds. Since the range of pixel values for a clear night sky is from 0 –16, it follows that the remaining range of pixel values has to be from thin clouds. In this study, we observe that the range of pixel values for thin clouds is from 19 –40. Fig. 1f is a histogram of an extreme example of a thick cloud where pixel values range from 47 –111. Visual inspection of Fig 1c shows that there is no thin cloud or clear sky component. This pixel range can represent of thick clouds at night time. This work has shown the possibility of discriminating cloud types in terms of the range of pixel values. In the future, these results will be used to calculate cloud cover from thin and thick clouds as the calculation of cloud occurrence is simultaneously done.

References:

Heinle, A., Macke, A., Srivastav, A. (2010). Automatic cloud classification of whole sky images. *Atmos. Meas. Teach*, 3: 557-567.

Gacal, G.F.B., Antioquia, C., Lagrosas, N. (2016). Ground-based cloud detection of night time clouds above Manila Observatory (14.64N, 121.07E) using a digital camera. *Aerosol and Air Quality Research. (submitted).*

Keywords: Digital image, Pixel values, Histogram, Nighttime clouds

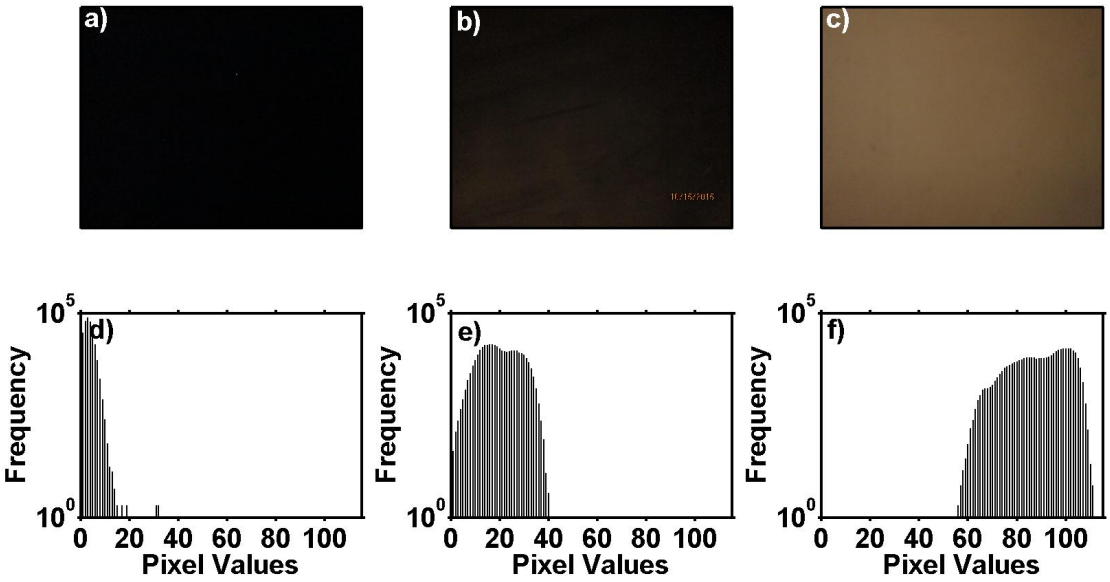

Observations of night time cloud cover sensitivity measurements with changes in threshold pixel values

*Nofel DelaCruz Lagrosas[1,2], Glenn Franco Barroso Gacal[1,2]

1.Manila Observatory , 2.Ateneo de Manila University

Detection of night time clouds is carried out in Manila Observatory (14.64N, 121.07E) for the purpose of measuring cloud cover at night time since late of 2014. A digital camera (Canon A2300 Powershot) is used to take images of sky every 5 minutes. Images are taken at 5s exposure time. The digital images, which are in standard RGB format, are converted to grayscale format for cloud detection analysis. Cloud detection is possible by setting a threshold pixel value that discriminates clear from cloudy sky. Previous study has shown that a threshold pixel value of 17 can be used for cloud detection (Gacal, et al, 2014). Cloud cover is defined as the ratio of the sum of the number of pixels identified as having cloud signals to the sum of the total number of pixels in the image. Cloud cover measurement has impacts on the radiation budget in the atmosphere even during night time. High cloud cover of thick clouds covering majority of the sky tend to reflect back radiation from the earth's surface. Thin clouds, on the other hand, may transmit earth's radiation to space and reflect less. In an ordinary image of night sky, the image may contain thick and thin clouds. In this work, we define a thick cloud in the image as cloud without any clear dark background. The images of thin clouds have visible dark background. For the purpose of quantifying cloud cover from thin and thick clouds, we present in this study the effects of varying threshold pixel value used in cloud detection algorithm on the calculation of night time cloud cover. Figs. 1a-c show images of clear sky, thin cloud and thick clouds taken on 12 January 2016 at 03:05, 22 December 2015 at 05:40 and 16 January 2016 21:15 local time, respectively. Local time is 8 hours ahead of coordinated universal time (UTC). Histogram of pixel values of clear sky image shows that maximum pixel value is 16 and can be used as a threshold value for discriminating clear from cloudy skies in the cloud detection algorithm. When this threshold value is changed from 10 to 40, cloud cover values also change. At threshold pixel value of 10, cloud detection algorithm applied to clear sky outputs ~3% cloud cover but rapidly decreases to zero for higher pixel values (Fig. 1d). When the algorithm is applied to thin cloud image, a sharp decrease of cloud cover values is observed for threshold pixel value > 20 but almost 100% cloud cover for threshold pixel value < 20 (Fig. 1e). From visual inspection of the image, a near 100% cloud cover is evident. The near exponential decrease of cloud cover values is a common characteristic when threshold pixel value is changed for images with thin clouds. Thus, without any idea of the image, this exponential decrease of cloud cover trend can be used to indicate that the image is dominated by thin clouds. When threshold pixel values are changed in the cloud detection algorithm and applied to images with thick clouds, the decrease of cloud cover values is not as sharp as in the case of thin clouds. Fig. 1f shows the non-exponential decrease of cloud cover values with threshold pixel value change. The graph shown is Fig. 1f is also a characteristic graph for thick clouds. Thus, the non-exponential decrease can be used for determining presence of thick clouds in the image without inspecting at the image. Images of rain clouds are extreme examples of thick clouds. When images of these types of clouds are processed using the same algorithm and changing threshold pixel value from 10 to 40, resulting cloud cover values do not change and are at 100%. This is expected since pixel values of thick clouds are usually in the range of 47 to 111.

Keywords: Night time clouds, Pixel value, Cloud cover

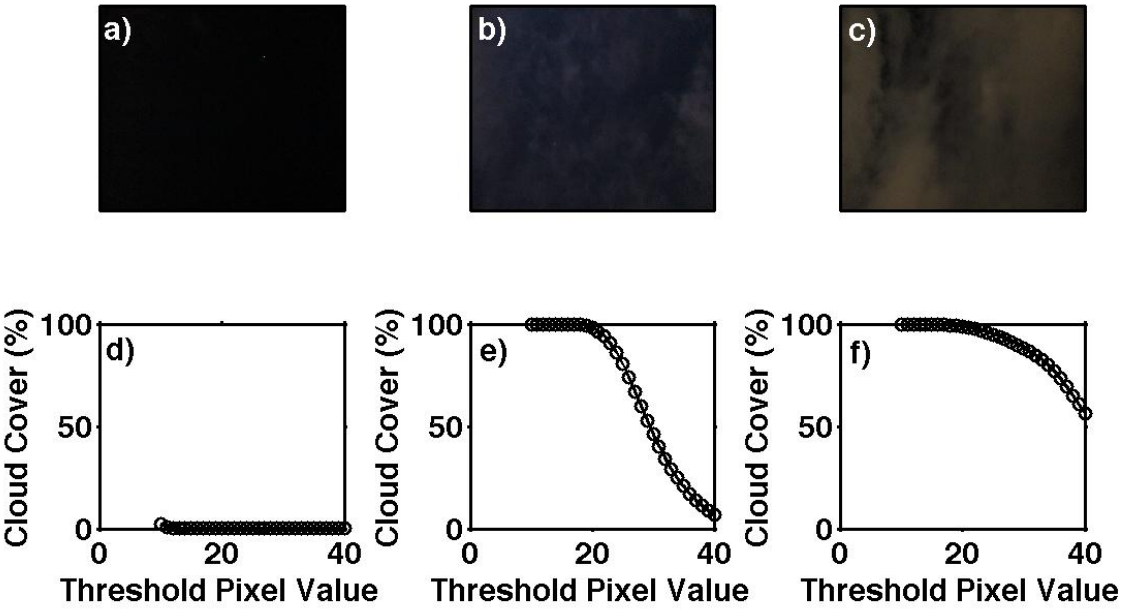

Three dimensional structure of the Arctic cyclones

*Takuro Aizawa[1], Hiroshi L Tanaka[2]

1.Graduate School of Life and Environmental Sciences, University of Tsukuba, 2.Center for Computational Sciences, University of Tsukuba

Arctic cyclones are unique low pressure systems appearing in the Arctic, which are different from the tropical cyclones and the mid-latitude cyclones. Previous studies provided a new insight that the surface Arctic cyclone connects to an upper polar vortex producing a deep barotropic vortex. The previous studies also noted that the characteristic thermal and the vortical structures are maintained throughout a life cycle. But, the three dimensional stereoscopic structure of the Arctic cyclones was not investigated by the previous studies.
To investigated the three dimensional structure of the Arctic cyclones, we converted the meteorological data from a latitude/longitude coordinate system into the cylindrical coordinate system around the Arctic cyclone center. The original data used this study are the reanalysis data of JRA-25 (Japanese 25year Reanalysis) and JRA-55 (Japanese 55year Reanalysis).
The Arctic cyclone has a deep barotropic cyclonic circulation, a secondary circulation in the troposphere, a downdraft at the lower stratosphere, a coupling of a warm core at the lower stratosphere and a cold core in the troposphere, and a deep tropopause folding over the cyclone center.
For the Arctic cyclone, the positive relative vorticity related to the deep axisymmetric cyclonic circulation stretches up to the stratosphere of 50 hPa level from the surface indicating a connection with the stratospheric polar vortex. The upper vortex of the well-developed occluded cyclone is not the polar vortex in the stratosphere. The Arctic cyclone at the surface is characterized by the deep stratospheric polar vortex, which is a different from the occluded cyclone in terms of the vertical scale.
Although additional studies are needed, a schematic diagram of the Arctic cyclone is proposed in this study.

Keywords: Primary circulation, thermal structure, polar vortex

An anaysis of fine structure in the summer troposphere and stratosphere based on radiosonde observations at Shigaraki, Shiga, Japan

*Yuta Mizutani[1], Shota Sugano[1], Yuki Kawata[1], Kaoru Sato[2]

1.Dept. Earth and Planetary Physics, School of Science, The University of Tokyo, 2.Department of Earth and Planetary Science, The University of Tokyo

In order to examine characteristics of atmospheric fine structure in the troposphere and stratosphere, radiosondes were launched every 3 hours from 18:00JST 27th July,2015 to 18:00JST 28th at Shigaraki MU Observatory, Kyoto University. Vertical profiles of horizontal wind, temperature, and relative humidity were obtained at a height interval of 5 m. During the observation period, high and low pressure systems are situated in the south and north of Japan, respectively. This is a typical synoptic-scale pressure pattern in summer in Japan. The tropopause determined based on the Brunt-Vaisala frequency was located around a height of 15 km. Using these observation data, time evolution of the atmospheric boundary layer, altitude dependency of dominant vertical wavelength, and dynamic characterictics of dominant wave-like structure in the stratosphere were analyzed.
First, we examined in detail the vertical profiles of the potential temperature, the equivalent potential temperature, and water-vapor mixing ratio to see development of the atmospheric boundary layer in daytime. It is expected that these quantities are constant in the vertical as a result of strong convection in the mixing layer. The altitude up to which these quantities are constant was raised from 0.5 km to 1.2 km during the time period of 9:00-15:00LST. On the other hand, a strong inversion layer appeared in the lowermost troposphere at 3:00LST.
Second, a wavelet analysis with a box-car type mother wavelet was carried out. The wavelet spectrum for each vertical profile of temperature, zonal wind, and meridional wind was calculated, and the mean spectrum for the entire period was obtained. It was clear that dominant wavelength depends on the altitude. It is approximately 1 km and 6 km for the lower (15-25 km) and middle (25-35 km) stratosphere, respectively. Because any drastic change in the Brunt-Vaisala frequency and background winds were not observed, it is inferred that the disturbance with the long vertical wavelength in the middle stratosphere was generated in the region far from, propagated horizontally toward and reached the observatory.
Phases of the dominant wave propagate downward, suggesting that the disturbance is due to an internal gravity wave propagating energy upward. Given a working hypothesis that the wave disturbance was an internal gravity wave, a hodograph analysis was carried out. First, the background wind was obtained as a linear least square fit for the vertical profiles of zonal and meridional winds above a height of 20 km. Deviation from the background wind was analyzed as the disturbance component. The hodograph of the disturbance component was approximated by an ellipse. The intrinsic frequency was estimated from the ratio of long to short axes of the ellipse. The horizontal wavenumber was determined from the dispersion relation of the internal gravity wave, using the estimated intrinsic frequency and the vertical wavenumber directly obtained from the vertical profile. The ground-based frequency that was determined from these wave parameters and the mean wind was approximately consistent with that observed in the time series of the vertical profiles. This means that the working hypothesis was valid and that the disturbance is due to an internal gravity wave. Furthermore, using these wave parameters and the mean wind, and the propagation paths of the internal gravity wave was estimated. As a result, it was concluded that the gravity wave likely originated from the low pressure system over a northern part of Korean Peninsula.

Keywords: radiosonde observations, wavelet analysis, internal gravity waves

Changes in the lower stratospheric residual circulation in JRA-55

*chiaki Kobayashi[1]

1.Meteorological Research Institute

Future projections by many climate models suggest that the Brewer-Dobson circulation (BDC) will be intensified as a result of rising greenhouse gas concentrations. However, observations show a diversity of the BDC strength changes. In this study, we investigate the changes in the BDC using JRA-55 reanalysis data compared with JRA-55-related products. In JRA-55, the annual mean tropical upwelling shows a significant increasing trend in the lower stratosphere from 1979 to 2012. JRA-55C also indicate a significant increasing trend of the upwelling, but JRA-55AMIP does not. These BDC strengths are assessed by climatological zonal mean which is removed diurnal variations.
Recently, Sakazaki et al (2015) found zonally uniform tidal signals in the tropical stratosphere. The vertical wind diurnal amplitudes in the lower stratosphere is not a negligible amount compared with climatological upwelling.
The BDC trend in JRA-55 linked with the representation of the tidal signals change related to the observing system changes in the reanalysis. Comparison of the relation among the JRA-55 family members is discussed in the presentation.

Keywords: JRA-55, Brewer-Dobson circulation, lower stratosphere

Characteristics of the polar vortex and the AO index in the upper stratosphere and lower mesosphere in Arctic winter II

*Kazuyo Sakanoi[1], Takenari Kinoshita[2], Kaoru Sato[3], Yasuhiro Murayama[2]

1.Komazawa University, 2.NICT, 3.The University of Tokyo

Purpose of this research is to clarify relationship between solar activity and disturbance in the middle atmosphere during Arctic winter. In this research we consider stratospheric sudden warming (SSW), which is a typical phenomenon in Arctic winter, as disturbance in the middle atmosphere including the mesosphere. Previous research [ex. Labitzke, 2005] reported effect of 11-year solar cycle on thermal structure only in the Stratosphere.
Traditional classification of SSW is not suited for quantitative comparison with other indices. Therefore we are exploring new indices which display condition of disturbance in the mesosphere. In this presentation, we calculate AO index in the altitude range from 1000 hPa to 0.1 hPa (65km alt) in 1999/2000 -2007/2008 winters. AO index also represents well the degree of disturbance in the middle atmosphere. We also use 2D vortex moment diagnostics (Z10 method) [Seviour et al., 2013] to check condition of the polar vortex at 10 hPa and 0.316 hPa. The results of these analysis is summarized as follows:
> The peak altitude of AO index is about 0.5 hPa.
> Positivity/negativity of AO index is almost coincident at 100 hPa -0.1 hPa.
> High negative value and negative AO index in all altitude are not necessarily required in Major Warmings.
> Wave 1 and 2 configuration are observed at 10 and 0.316 hPa in Major Warmings and comparable level events. Strong wave 1 is exists especially in 10 hPa.
> Wave 1 and 2 configuration are observed at 0.316 hPa in minor Warmings. At 10 hPa there are no disturbance or wave 2 configuration.
> Negative AO is shown in all altitude range when strong wave 2 exist at 10 hPa.
References:
Labitzke, K. (2005). On the solar cycle-QBO relationship: A summary. Journal of Atmospheric and Solar-Terrestrial Physics, 67(1-2), 45-54. http://doi.org/10.1016/j.jastp.2004.07.016
Seviour, W. et al. (2013). A practical method to identify displaced and split stratospheric polar vortex events. Geophysical Research Letters, 40(19), 5268-5273. http://doi.org/10.1002/grl.50927

Keywords: Stratospheric sudden warming, Arctic, Mesosphere

Dynamical response of the SH middle atmosphere to energetic particle precipitations in the latest reanalysis data

*Yoshihiro Tomikawa[1,2]

1.National Institute of Polar Research, 2.SOKENDAI

The latest solar cycle minimum sometime around 2009 showed unusually low solar activity and suggested the possibility of a grand solar minimum in the near future. This event caused much attention to be focused on studies regarding solar influence on the Earth's climate. The recent review by Gray et al. (2010) classified solar forcing on the Earth's climate to be of four types: galactic cosmic rays, total solar irradiance (TSI), solar ultraviolet radiation (UV), and energetic particle precipitations (EPP). Although EPP has not attracted much attention compared with TSI and UV in the past, several recent studies indicate that EPP could have a significant impact on the Earth's climate, comparable with that of TSI and UV. However, reliability of some of these studies was recently questioned (Tomikawa, 2015). In this study, the past 36 years were divided into high, medium, and low energetic particle forcing (EPF), and solar maximum, medium, and minimum conditions using Ap index and F10.7 radio flux, respectively. Then composite figures of middle atmosphere in the winter southern hemisphere were created from the latest reanalysis data and compared between medium and low EPF during the solar minimum. They showed that there was a statistically significant difference between medium and low EPF.

Keywords: Energetic particle precipitation, Reanalysis, Middle atmosphere

An observation of the mesospheric column amount of nitric oxide observed with a millimeter-wave spectral radiometer at Syowa station in Antarctica

*Tomoo Nagahama[1], Akira Mizuno[1], Tac Nakajima[1], Hirofumi Ohyama[1], Yasusuke Kojima[1], Mitsumu K. Ejiri[2], Yoshihiro Tomikawa[2], Masaki Tsutsumi[2], Takuji Nakamura[2]

1.Institute for Space-Earth Environmental Research, Nagoya University, 2.National Institute of Polar Research

Since 2011, the ISEE and NIPR started a joint research project on monitoring the composition changes in mesosphere and lower thermosphere (MLT) by using a millimeter-wave spectroscopy technique, and installed a millimeter-wave spectral radiometer with a high-sensitivity superconducting (SIS) mixer receiver operated in 250 GHz band at Syowa station in Antarctica (69°S, 40°E) for measuring the emission spectrum of nitric oxide (NO) in January 2012. The partial column of NO ranging from 75 to 100 km in altitude is retrieved from the observed emission spectrum. The mesospheric chemical composition largely varies caused by environmental changes of the earth inside and outside. Recent studies reported enhancement of NO_x and HO_x and ozone depletion in the polar mesospheric region caused by precipitating the energetic particles such as a solar proton and an electron in the radiation belt (e.g., Andersson et al. 2014). From the dataset observed with the radiometer in more than 4 years, we find that the NO column amount shows the maximum in winter, but the peak amount in 2014 is about a half of those in other years. In addition, we detect sporadic enhancement of the NO column amount during a few weeks in June, August and October of 2015 that may be associated with solar activity. In the presentation, we report the features of temporal variations of the observed NO column amount as well as the detail comparison with physical properties of precipitating solar protons and the electrons from the radiation belt.

Keywords: mesosphere, atmospheric composition change, millimeter-wave measurement

Influences of QBO and solar cycle on the Arctic ozone

*Yousuke Yamashita[1], Hideharu Akiyoshi[1]

1.National Institute for Environmental Studies

The quasi-biennial oscillation (QBO) and the solar 11-year cycle are known to cause year-to-year variability of the Northern Hemisphere (NH) polar vortex (e.g., Holton and Tan, 1980; Labitzke and van Loon, 1988). Yamashita et al. (2015) indicated that the polar vortex is strong in early winter and weak in late winter for the westerly phase of the QBO (QBO-W) and solar maximum (S_{max}) years. In contrast, the polar vortex is strong from early to late winter for the QBO-W and solar minimum (S_{min}) (QBO-W/S_{min}) years, implying the small Arctic ozone in late winter. Li and Tung (2009) found that the observed Arctic total ozone in March is the smallest in magnitude for the QBO-W/S_{min} years. In this study, the influences of QBO-W/S_{min} on the Arctic ozone in late winter are analyzed from outputs of a chemistry climate model (CCM) in which the meteorological fields of the model are nudged toward the observational data for 1979–2011. The strong polar vortex relative to the climatology is shown in February–March during QBO-W/S_{min}. The minimum of Arctic total ozone is simulated during the QBO-W/S_{min} condition in February–March, in agreement with the satellite observations. We also analyze the total ozone derived from passive ozone tracer that is simply advected without any chemical change. The results of the passive ozone tracer show the similar results of the original total ozone, suggesting the prominence of transport change of ozone for the minimum total ozone under the QBO-W/S_{min} condition in February–March. The further analysis of the vertical structure suggests that while the minimum of Arctic total ozone is mainly explained by the transport change of ozone around 100–200 hPa, the enhancement of chemical destruction of ozone due to the low temperature within the polar vortex observed around 20–50 hPa under the QBO-W/S_{min} condition is partly related to the local ozone depletion around 20–50 hPa.

Keywords: quasi-biennial oscillation, solar 11-year cycle, Arctic ozone

A global analysis of seasonal total ozone trend for the CFC increase period using TOMS data and the MIROC3.2 nudged Chemistry-Climate Model

Risa Obama[1], *Hideharu Akiyoshi[1], Yousuke Yamashita[1], Masanao Kadowaki[1]

1.National Institute for Environmental Studies

In this study, we globally analyzed seasonal total column ozone trends for the period 1979-1993 and 1979-1997. We compared the total ozone trends of a nudged CCM with those of TOMS. The nudged CCM is the MIROC3.2 Chemistry-Climate Model nudged toward ERA-Interim reanalysis data. The comparison showed that the model simulation reproduced well the trends globally. In order to separate the effects of ozone changes due to the chemical reactions and the transport on the trends, we performed a 1979-ODS experiment, in which ODS concentration was fixed to the 1979 value. The results indicate that chemical ozone loss is more dominant as a driver of the trends than ozone transport change at the mid-latitudes in the Southern Hemisphere, whilst at the mid-latitudes in the Northern Hemisphere ozone transport is more dominant than the chemical loss in the winter and spring, and both the effects are comparable in the summer and autumn. From a global ozone trend map, we show significant negative trends over the Pacific Ocean in the east of Japan, around the east coast of the North America, and over Europe. These trend distributions suggest some effect of planetary scale wave activitiy change in the Northern Hemisphere winter and spring for the CFC increase period.

Keywords: total ozone, long-term trend, nudged Chemistry-Climate Model, TOMS, ERA-Interim

Variations of stratospheric and tropospheric circulations related with ozone hole

*MASAAKI NAKAMURA[1], MASAAKI TAKAHASHI[2], HIDEHARU AKIYOSHI[3], Yousuke Yamashita[3]

1.Mitsubishi UFJ Research and Consulting, 2.Atmosphere and Ocean Research Institute, University of Tokyo, 3.National Institute for Environmental Studies

Due to anthropogenic emissions of ozone depleting substances, ozone hole has been developing in Antarctic stratosphere during the spring since about the 1980s. Ozone absorbs incoming solar radiation and heating the stratosphere. Hence the depletion of ozone over Antarctica leads to cooling of the polar stratosphere. As a result, polar vortex is strengthened from thermal wind equation. These variations related with ozone hole appear only in Antarctic stratosphere during the spring so that it was considered that the ozone depletion does not affect tropospheric climate. Since about the 2000s, however, it has become clear that the ozone hole is also associated with widespread changes in the Southern Hemisphere tropospheric circulation and surface climate. Previous research studies showed that the influences of the ozone hole go down from stratosphere and appear lower troposphere during the austral summer season. This tropospheric variation pattern resembles the most prominent pattern of large-scale Southern Hemisphere climate variability, the Southern Annular Mode. Hence the influence of the ozone hole has led to a range of Southern Hemisphere climate changes not only Antarctic stratosphere, but also over the Southern Hemisphere troposphere. However the mechanism of influence from the stratosphere to the troposphere is unclear. This study revealed how the stratospheric variation related with ozone hole affect the troposphere during austral summer season.

Previous study analyzed this mechanism using monthly or seasonal data; therefore, variations with timescale shorter than a month cannot be analyzed. For this reason, we used 10 days mean data in order to research the detail of the mechanism in the austral summer. As a result, we found out the variations of eastward wind are different among December, January and February. In December, most of eastward wind variations occur in the stratosphere and upper troposphere. In January, stratospheric variations disappear and only tropospheric variation can be found. In February, we could not find any significant variations both stratosphere and troposphere. We tried to find out the reason why these different variations appear using EP-Flux. As a result, we realized that, in December, wavenumber 1 propagating into the stratosphere has the most important role and that baroclinic instabilities with wavenumber 4 and 6 are important in January.

Furthermore we studied the influences of both global warming and ozone hole on Southern Hemisphere climate. We investigated in the Chemical Climate Model based on MIROC 3.2 using three scenarios, one is reference simulation, another is sensitivity simulation which is similar to reference simulation, but halogens fixed at 1960 levels throughout the simulation, and the last is sensitivity simulation which is also similar to reference simulation, but GHGs fixed at 1960 levels. Hence we can discuss two influences both global warming and ozone hole on Southern Hemisphere climate variations separately. As a result, we realized ozone hole has a role to maintain the signal at the lower troposphere in austral summer. On the other hand, global warming makes Brewer-Dobson circulation strong and the transportation of ozone to polar region is also enhanced. Because of ozone heating, global warming has a role to warm the polar atmosphere. Previous studies notice only the GHGs`s radiative cooling in the stratosphere but we suggested that the change of physical field is also important in the variation of Southern Hemisphere climate.

Un-volatile aerosol layer in the lower most stratosphere over tarawa, Kiribati, observed bu balloon norne Optical Particle Counter in january, 2016

*Masahiko Hayashi[1], Naomi Eguchi[1], Koichi Shiraishi[1], Yoichi Inai[2], Satoru Mimura[2], Fumio Hasebe[2], Takashi Shibata[3]

1.Faculty of Science, Fukuoka University, 2.Hokkaido University, 3.Nagoya University

Size distributions and volatility of aerosols in the Tropical Tropopause Layer (TTL) over Tarawa (1.5 °S, 173.0 °E) were observed using balloon-borne dual optical particle counters (OPC) in January 2016. One OPC observed number concentration of ambient aerosols and another OPC observed aerosol size distribution denuded at 200 °C, in order to discuss volatility of aerosls.
Unusual aerosol layer was found in the stratosphere from 18 to 22 km in altitude. The layer was divided into two sub-layers. Upper layer was characterized by smaller high volatile aerosol, and lower one by mixture with larger submicron un-volatile aerosol. The feature was similar to fresh volcanic aerosol layer, however we did not find any report of large volcanic eruption in 2015. We will discuss about origin of the layer.

Keywords: Tropical Tropopause Layer, stratsphere, aerosol, volatility

